Journal of Engineering and Sustainable Development
Vol. 30, No. 05, August 2026
https://jeasd.uomustansiriyah.edu.iq/index.php/jeasd
ISSN 2520-0917
Research Article
https://doi.org/10.31272/jeasd.2797

Compact Tri-band Half-Mode Substrate Integrated Waveguide Loaded by Meandered Slot Line for Wireless Communications

Hasan AL-Darraji*, Hussam AL-Saedi

Communication Engineering Department, University of Technology, Baghdad, Iraq

*Email: coe.21.21@grad.uotechnology.edu.iq

Article Info

Received	**19/06/2024**
Revised	**08/08/2026**
Accepted	**08/08/2026**

Abstract

This paper presents the utilization of a half-mode substrate integrated waveguide (HMSIW) cavity loaded with a meandered slot line (MSL) to design a miniaturized a 2nd order tri-band bandpass filter (BPF). The MSL was employed to independently control the operating passbands and to reduce the filter size. A systematic design procedure was used in this work to systematically calculate the theoretical parameters. Ansys EDT and ADS simulators were adopted to design and optimize the proposed structure and validate the achieved results. Simulation results showed that the proposed filter occupies an area of $0.041\lambda_g^2$ at 4.7 GHz acquiring a compact size. Simulation results showed that the optimized structure operates with three passbands centred at 4.7 GHz, 7.28 GHz, and 9.36 GHz with insertion losses of 0.23 dB, 0.77 dB, and 1.8 dB, and the return losses of 20 dB, 19 dB, and 18 dB, respectively. The achieved findings showed that the proposed filter is compact and exhibits superior performance, which makes it well-suited for emerging multi-functionality wireless communication applications. The filter's size reductions and tri-band functionality make it a particularly desirable option for integration within miniaturized communication systems.

Keywords: Bandpass Filter, Half-Mode, Meandered Slot Line, Multi-Band, Substrate Integrated Waveguide.

1. Introduction

The need for high-performance bandpass filters (BPFs) with compact size and multiple standards is increasing, especially for wireless communication. Several technologies, such as planar, microstrip, and Substrate Integrated Waveguide (SIW), can be employed to implement such filters [1]-[2]. SIW technology provides low-loss structures that handle high power well, but size remains a challenge and requires further study and improvement [3]. Modern wireless systems, including 5G, 6G, and beyond, rely on multi-band operation to provide users with high data rates and low latency [4], [5]. Consequently, in these applications, the multi-band operation can be a crucial component [6], [7]. Several researchers, including [8]-[26], implement SIW technology to realize multi-band BPFs and Dual-band (DB) BPFs [8]-[14]. Another study suggested an E-slot applied on SIW to get a DB BPF working with center frequencies of 3.6 and 6.4 GHz with an overall area of $0.084\lambda_g^2$ [8]. A different topology, such as a complementary split ring resonator (CSRR), was implemented on SIW to generate a second-order DB BPF working at center frequencies in the first band of 7.89 GHz and the second band of 8.89 GHz through excited modes (TE_{102} and TE_{201}); the suggested filter was constructed on a relatively large area of $0.74\lambda_g^2$ [9]. A single resonator was designed to generate a DB BPF operating at 7.71 and 9.64 GHz as the center frequencies, using circular SIW technology with via posts and slots loaded on the suggested resonator. The overall area was $1.25\lambda_g^2$ which is relatively large. A higher-order filter is difficult to realize, and the unused area between the resonators increases [10]. A multi-layer SIW technology used to implement DB BPF working on center frequencies of 9.2 and 12.2 GHz with a large working area of $1.4\lambda_g^2$. Hence, this type of technology requires complex fabrication steps, which lead to increased overall costs [11]. Another study that relies on DB BPF, reported in [12], focuses on center frequencies of 8 and 11.4 GHz. A third-order dual-band BPF was realized using dual- and single-mode SIW resonators; although this design achieves wide stopband rejection, the overall size remains immense. $2.17\lambda_g^2$.

A second-order DB BPF was realized by utilizing various diameters of vias; the center frequencies were (17.1 and 19.38) GHz, and the overall size was relatively large. $2.64\lambda_g^2$[13].

A circular SIW resonator was stacked to develop a dual BPF by Zhu et al. [14]. The third-order filter operates at 9.89 and 11.98

GHz but requires three substrates, making the structure complex. The works presented in [8]-[14] focused on designing a dual-band BPF based on SIW technology; most of these structures occupy a large filter area, and some designs require a multi-layered stack-up. Furthermore, the works in [15]-[17] proposed SIW structures to generate Dual- and tri-band BPF responses. A rectangular SIW resonator with post vias was used to design a DB BPF, and stacked extra SIWs were used to modify this filter to generate a tri-band (TB) BPF [15]. The TB BPF operating at 6.5 GHz, 7.35 GHz, and 8.15 GHz was implemented with a dual-layered stack over an area of 1.08 1 over lambda g subscript basere of 1.08 $1/\lambda g.\lambda_g^2$. In [16] DB, TB, and quad-band (QB) BPFs were proposed by employing a multi-mode SIW resonator associated with CSRRs. The TB BPF operates at 7.55, 9.3, and 10.81 GHz with a filter area of 1.06 lambda sub g squared. A stacked multi-layered SIW was used in [17] to design a DB and TB BPF. The TB BPF uses triple substrates coupled with slots, making it a complicated structure.

Triple-band BPFs were proposed in [18]-[21]. A fourth-order filter was generated in [18] by integrating a via post within a triple-mode resonator and a grounded coplanar waveguide (GCPW), and delivers a quasi-elliptical response at 11, 12, and 13 GHz, though it spreads over a very large 4.84 λ_g^2. A square SIW resonator forms the basis of [19], perturbed by slots and via posts to obtain a triple-band response; the filter works at 16.9, 17.5, and 21.3 GHz within 2.07 λ_g^2. In [20], three circular SIW resonators are stacked vertically to exploit the evanescent mode, producing a TB BPF at 1.83 GHz, 2.1 GHz, and 2.47 GHz in only 0.048 λ_g^2. The area is remarkably small, but the complex multilayer configuration remains a drawback. Li et al. [21] reported the utilization of a magnetic coupling within triple modes stacked SIW resonators for a TB BPF at 11.92 GHz, 13.23 GHz, and 14.1 GHz, where metallic vias perturb a square SIW resonator to generate the triple mode; two stacked substrates bring the area to 2.72 λ_g^2. Like the works in [9]-[18], those in [18]-[21] are limited by size, and several depend on complex multi-layer stacks. All of [8]-[21] build on full-mode SIW resonators, which is why a large size is needed to obtain the required response.

Mode splitting, in the form of half-mode (HM), three-fourths-mode (TFM), and quarter-mode (QM) resonators, was applied in [22]-[24] to implement miniaturized tri-band SIW BPFs. In [22], an HMSIW resonator loaded with a modified E-shaped defected ground structure yields a second-order TB BPF at 12.7, 20.7, and 28.6 GHz. Its fabricated area is a compact 0.12 λ_g^2, although the feed lines belong to the filter structure and add to the overall size. The tri-band BPF in [23] is centered at 2.1, 3.98, and 6.6 GHz and is built from a QM circular SIW resonator loaded with an arc-like slot and an open-ended stub, with lumped capacitors improving the impedance matching; it occupies 0.05 λ_g^2. A rectangular SIW cavity resonator operating in its TFM was adopted in [24] for a second-order tri-band BPF at 3, 4.24 and 5.24 GHz, taking up 1.07 λ_g^2. This state-of-the-art shows that multi-band SIW BPFs are a promising solution for modern wireless communication systems, while size and complexity remain drawbacks that call for further research.

Accordingly, this paper presents the design, optimization, and validation of a miniaturized 2nd-order tri-band HMSIW BPF. The main objective of this paper is to develop a compact tri-band bandpass filter that can be utilized in modern wireless communication systems. Moreover, the proposed filter operates with three bands that can be adjusted independently so that any arrangement may be realized. The HMSIW cavity resonator was loaded with a meander-shaped slot line to perturb the first three modes (namely TE_{101}, TE_{102}, and TE_{201}) independently and miniaturize the proposed structure. The filter was simulated using Ansys EDT 2022 R1, and its performance was validated through the utilization of the Advanced Design System (ADS) 2020 simulator. Excellent agreement between the results of both simulators over the entire operating frequency makes it suitable for modern wireless communication systems.

2. Method of the Research

2.1 Proposed Filter Design Procedure

The design procedure and analysis of the proposed filter are introduced in this section. First, the development of the HMSIW resonator loaded with a meandered-shape slot line is suggested theoretically, and a full-wave simulator is used to study its behavior. Second, a systematic design procedure is followed to construct the main components of the proposed filter. Parametric studies were performed to optimize the parameters of the suggested structure. Finally, the complete filter structure is presented.

SIW technology provides high-performance resonators and passive circuits, including filters, antennas, splitters, and beam forming; however, such devices are constructed with a large area, limiting the usability of this technology in compact and portable systems. Therefore, this paper proposes a well-organized methodology to overcome the addressed problem. Furthermore, modern communication systems function over multi-band and acquire BPFs operating with different passbands with specific bandwidths, so a space-filling MSL is suggested to allow an independent control mechanism over these bands. An SIW rectangular cavity resonator can be treated as a dielectric-filled standard rectangular waveguide (RWG), assuming that leakage losses are insignificant, where the design equations of the latter are utilized to calculate the resonance frequencies of the propagating modes [25]. The resonance frequency of the TE_{m0q} mode in an RWG filled with dielectric can be calculated by equation (1).

$$f_{TE_{moq}} = \frac{c}{2\sqrt{\mu_r \varepsilon_r}} \times \sqrt{\left({}^{m}/_{W}\right)^2 + \left({}^{q}/_{L}\right)^2} \qquad (1)$$

Where W and L represent the width and length of an RWG, respectively, m and q are the mode numbers in the x- and y-axis directions, respectively, and c is the speed of light in vacuum. Moreover, the dimensions of the SIW resonator are determined by applying equations (2-4).

$$P \leq 2d \qquad (2)$$

$$w_{eff} = W - \frac{d^2}{0.95 \times P} \qquad (3)$$

$$l_{eff} = L - \frac{d^2}{0.95 \times P} \tag{4}$$

Where W_{eff} and L_{eff} denote the effective width and length of a full mode (FM) SIW resonator, d is the diameter of the via hole, and P is the pitch (distance between consecutive via holes). A low-cost and industry-adopted substrate from Rogers Inc. (RO4003C) was used in this work; it has a relative permittivity (ε_r) of 3.55 and a dielectric loss tangent (tan δ) of 0.0027 with substrate thickness (h) of 0.508mm. The dimensions of the SIW resonator were assigned to be W = 7 mm, L =7 mm, d = 0.25 mm, and P = 0.5 mm. To evaluate the resonance frequencies of the TE_{101}, TE_{102}, and TE202 modes, eigenmode simulation was utilized. It is found that these modes resonate as follows: TE_{101} at 16.07 GHz, TE_{102} at 25.19 GHz, and TE_{202} at 25.53 GHz, with an unloaded quality factor (Q_u) of 370 for all modes.

The first step towards size reduction was to design an FMSIW resonator that was cut in half along its symmetrical magnetic wall, creating a HMSIW resonator; hence, this process effectively halves the resonator size. HMSIW cavity design is an innovative approach that significantly reduces the width of traditional SIW structures by half while maintaining their advantageous properties, such as low loss, high power handling capability, and ease of integration with planar circuits. The resultant HMSIW resonator is capable of accommodating the $TE_{0.5,0}$ mode. The width of the HMSIW ($W_{eff,\ HMSIW}$) and the cut-off frequency can be determined using equations 5 and 6, respectively [26].

$$W_{eff,HMSIW} = \frac{W_{eff}}{2} \tag{5}$$

$$f_{c_{TE0.5,0}} = \frac{C}{4W_{eff,HMSIW}\sqrt{\varepsilon_r}} \tag{6}$$

The dimensions of the HMSIW resonator are W_{HMSIW}=3.5 mm and L=7 mm.

The second step to further miniaturize the suggested HMSIW resonator was achieved by incorporating a slot line. A space-filling technique such as meandered curvature was adopted in this work to effectively utilize the space on the top metallic layer. The proposed HMSIW resonator loaded with a meandered slot line (MSL) is depicted in Fig. 1 (a-b), where the design parameters are highlighted.

The MSL dimensions were set (A1, A2, A3, A4, A5, B1, B2, B3, B4, and S) to (2.06, 2.6, 1.45, 0.77, 0.32, 2.75, 2, 1.1, 0.57, and 0.1); all dimensions are in mm. With these values, three resonance modes appear, and each of them can be tuned quasi-independently through the same set of parameters. In the eigenmode simulation, the first three modes are excited at 5.4, 7.61, and 9.56 GHz, with unloaded quality factors of 452, 447, and 435. The electric-field distribution over the suggested resonator at these working center frequencies is shown in Fig. 2(a-c). The effect of the MSL on the modes is clear: compared with a conventional HMSIW resonator, the first mode shifts down from 16.07 GHz to 5.4 GHz, the second from 25.19 GHz to 7.61 GHz, and the third from 25.53 GHz to 9.56 GHz.

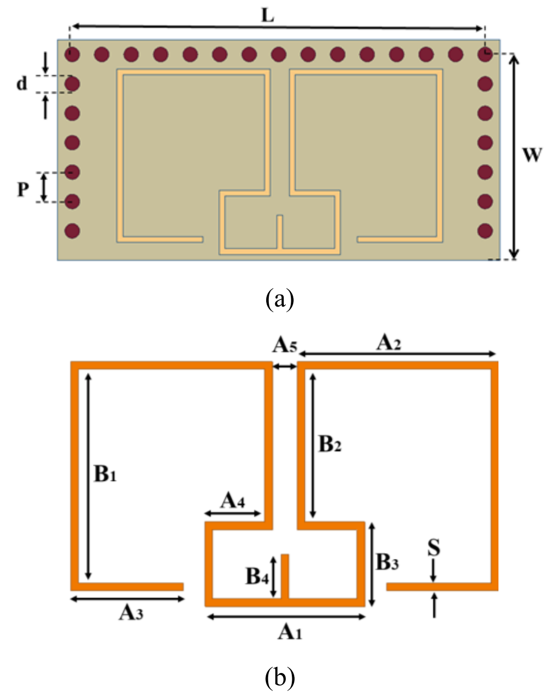

Figure 1. Suggested HMSIW loaded by a meandered slot line (a) Resonator and (b) MSL.

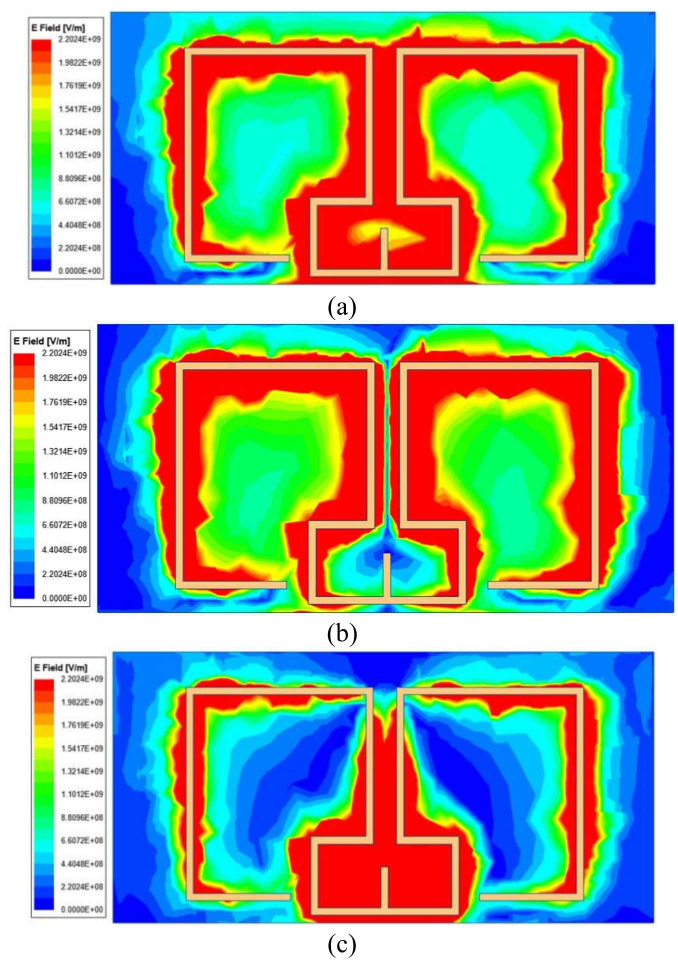

Figure 2. Simulated Electric field at the operating frequencies (a) 5.4 GHz, (b) 7.61 GHz, and (c) 9.56 GHz.

To study the effect of the dimensions of the MSL, an intensive full-wave simulation was conducted on the suggested HMSIW. The first step was ranged the parameter B_1 from 1 to 2.7 mm as shown in Fig. 3(a), by inspecting the attend results, a significant shift occurred on all resonance modes, e.g. mode 1 was shifted from 7.4 to 5.4 GHz; Moreover, a significant shift as compared to the first and third modes was realized on the second mode where the resonance mode moved from 10.44 to 7.4 GHz. Furthermore, a frequency shift from 10.94 to 9.18 GHz was obtained in the third mode, which was the lowest variation. As a result, a significant miniaturization can be performed by utilizing B_1.

The second parametric study was performed on the variable B_2. The simulation results revealed that the first resonance mode varied from 8.85 to 7.74 GHz as B_2 increased from 0.5 to 2 mm; in addition, the second resonance mode remained almost constant for the same B_2 variation interval. Moreover, a frequency shift from 11.45 to 11 GHz was observed in the third resonance mode, as demonstrated in Fig. 3(b).

A third parametric study applied on B_3 where increased from 0.6 to 1.2 mm with step size of 0.1 mm. the second and third modes experienced the most affect as compared to the first mode, which it stayed unchanged within B_3 interval as depicted in Fig. 3(c). the second resonance mode dropped from 8.65 GHz to 7.36 GHz; similarly, mode 3 decreased from 10.94 GHz to 9.15 GHz

Fig. 3(d) displays the impact of varying A_4 of (0.4-0.9) mm on the resonance modes of the proposed structure. It can be noted that the first resonance mode almost stayed fixed as A4 varies, while a frequency drop from 8.28 GHz to 7.35 GHz and 10.87 GHz to 9.15 GHz was achieved on the second and third resonance modes, respectively.

Based on the above-mentioned parametric study analysis, it can be concluded that a quasi-independently multi-mode resonator can be tuned effectively by incorporating an MLS on the top of the SIW resonator. Inspecting Fig. 3(c) and Fig. 3(d) confirms this conclusion, where in both figures the first resonance mode stayed almost constant while the second and third modes were changed significantly.

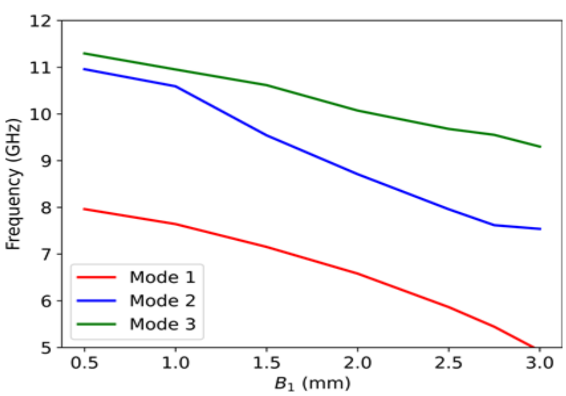

(a)

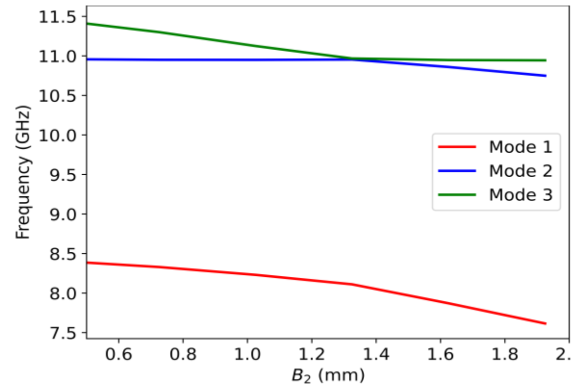

(b)

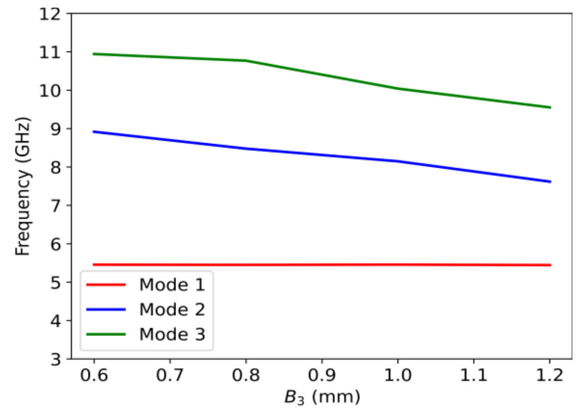

(c)

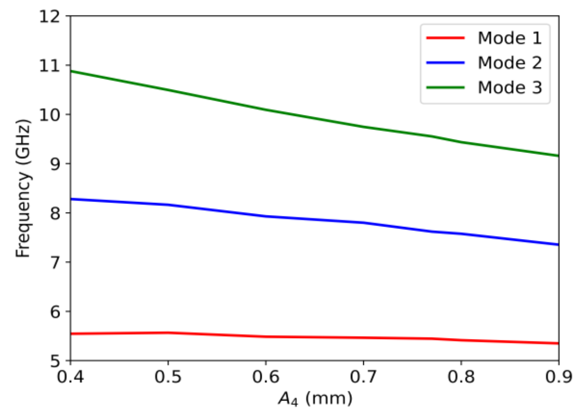

(d)

Figure 3. The impact of the MSL parameters on the operating frequencies (a) B_1, (b) B_2, (c) B_3, and (d) A_4.

2.2. Tri-band BPF Design Methodology

The insertion loss method was employed in conjunction with the superposition theorem to determine the required parameters of the lowpass filter prototype and the equivalent BPF for the three passbands. Equations (7-14) were employed to calculate the g-values for each band with Chebyshev response [27].

$$\beta = \ln\left(\coth\left(\frac{L_{AR}}{17.37}\right)\right) \tag{7}$$

$$\gamma = \sinh\left(\frac{\beta}{2n}\right) \tag{8}$$

$$a_k = \sin\left[\frac{(2R-1)\pi}{2n}\right], \quad R = 1,2,\dots,n \tag{9}$$

$$b_k = \gamma^2 + \sin^2\left(\frac{R\pi}{n}\right), \quad R = 1,2,\dots,n \tag{10}$$

$$g_o = 1 \tag{11}$$

$$g_1 = \frac{2a_1}{\gamma} \tag{12}$$

$$g_k = \frac{4a_{R-1}a_R}{b_{R-1}g_{R-1}} \tag{13}$$

$$g_{n+1} = \begin{cases} 1 & n\ odd \\ \coth^2\left(\frac{\beta}{4}\right) & n\ even \end{cases} \tag{14}$$

Where n is the filter's order, L_{AR} is the ripple level in the passband that can be calculated from the required return loss (RL). In this paper, a 2nd order tri-band centered at 4.7 GHz, 7.28 GHz, and 9.36 GHz with fractional bandwidths (FBWs) of 17.08%, 5.79 %, and 2.46 %, respectively, and RL= 20 dB was proposed; hence, based on (7-14), the calculated g-values were determined as shown in Table 1.

Table 1. Calculated g-Values of The Proposed BPF.

parameter	Value
g_o	1
g_1	0.66
g_2	0.54
g_3	1.22

2.3. Inter-Resonator Coupling

The second stage of BPF synthesis is to realize the theoretical coupling matrix by controlling the power flow from one resonator to its neighbor. This can be achieved by implementing via walls between every two resonators with a specific opening (G) within the wall, as shown in Fig. 4. The coupling factor can be calculated by employing Eigenmode analysis built into the Ansys EDT full-wave simulator.

In Eigenmode, two of the proposed resonators were built with a via wall in between to calculate the two degenerated modes, namely (f_e and f_m), electric and magnetic resonance frequencies, respectively, that represent the resonance frequency when an electrical and magnetic symmetrical wall is interpreted. By employing equations (15) and (16), the coupling coefficients (K) and Coupling matrix (M) can be calculated based on the values of fe and fm obtained from Eigenmode simulations when G is varied.

$$K = \frac{fe^2 - fm^2}{fe^2 + fm^2} \tag{15}$$

$$M = \frac{f_0}{BW} \times \frac{fe^2 - fm^2}{fe^2 + fm^2} \tag{16}$$

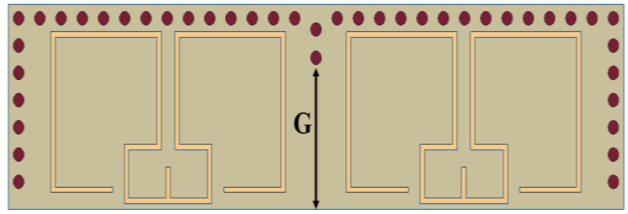

Figure 4. Inter-resonator coupling setup.

To realize the specified tri-band BPF response, the coupling matrix [**M**] for the three passbands was found as illustrated in Table 2.

Table 2. Coupling Matrix [M].

parameter	value
M_{11}	0
M_{12}	1.658
M_{21}	1.658
M_{22}	0

Eigenmode analysis was used to find the opening (G) that gives the required coupling coefficient (M_{ij}). G was swept from 0.5 mm to 3 mm, and the resulting M_{ij} is plotted in Fig. 5. M_{ij} rises as G increases, and G = 2.36 mm was selected as the optimal value, since it delivers the required M_{12} = 1.65.

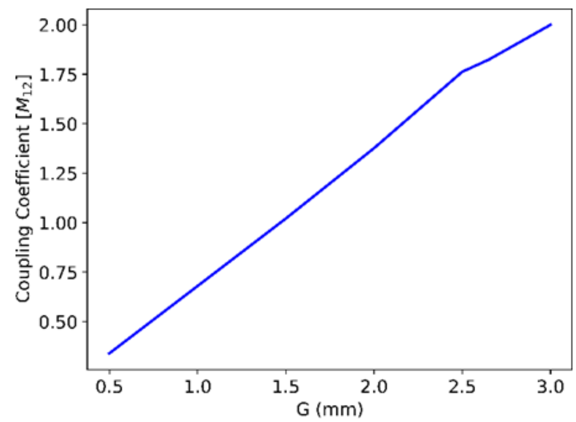

Figure 5. The relation between G in (mm) and M.

3. Input/Output Coupling

Group delay (τ) method can be utilized to properly couple the input/output resonators of the filter to other devices and allow the required frequencies to pass through the filter and reflect the unwanted frequencies. This approach is based on the examination of the group delay of the reflection coefficient S_{11}, and τ reaches its highest value at resonance when $\omega = \omega_o$. Equation (17) relates the maximum τ to the external quality factor (Q_e) of a resonator.

$$\tau_{max} = \tau(\omega_o) = (4Q_e/\omega_o) \tag{17}$$

Furthermore, the relationship between Q_e and the normalized impedance Z_o of the coupling matrix is calculated as [27]:

$$Q_e = {}^{\omega_0}/_{[\mathrm{Zo} \times (\omega_2 - \omega_1)]} \tag{18}$$

To excite the proposed BPF with the required power, the coupling between the feeding line and the input and output resonators must be optimized to achieve the required group delays within the operating passbands. The group delays can be analytically calculated by employing equations (17) and (18), where it is found that the required group delays in the proposed design are τ_1=0.53 ns, τ_2 =1.01 ns, τ_3 =1.84 ns. One of the most common methods to control the group delay of an SIW resonator fed by a microstrip line is to utilize an inset feed slot.

Fig. 6 depicts the proposed connection between the feed microstrip line and the suggested HMSIW resonator, where the width and length of the inset feed (WS and Lt) were optimized at compromised dimensions to achieve the best group delays compared to the theoretical values obtained from equations (17) and (18). Fig. 7 illustrates the simulated group delay versus frequency, which shows that the first group delay τ = 0.27 ns, the second group delay τ = 2.02 ns, and the third group delay τ = 3.45 ns; by comparison between the theoretical and the simulated group delays, it can be noticed that the difference at the first band was lowest and at the third band was the highest. As a result of these differences, it is expected that the first band will possess the narrower bandwidth with lower IL; nevertheless, the third operating band will experience a wider operating band and worse IL.

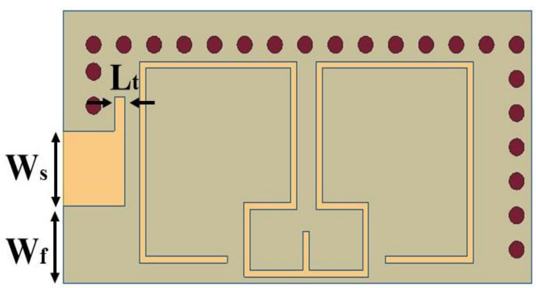

Figure 6. Group delay simulation setup.

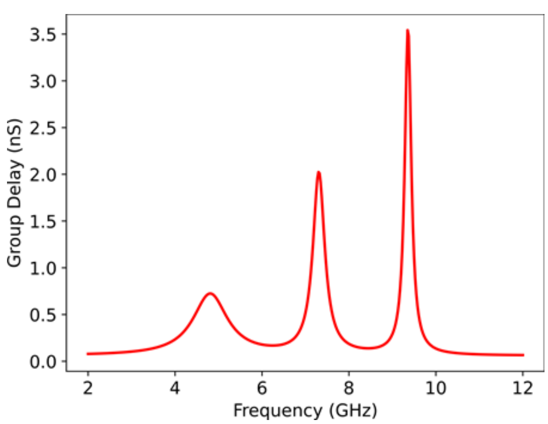

Figure 7. Simulated group delay vs. frequency in GHz.

4. Results and Discussion

Following the optimization of the resonator, coupling sections, and feeding structure, the complete tri-band filter was finalized, as depicted in Fig. 8. The optimized geometrical parameters of the proposed design are summarized in Table 3. Owing to the compact HMSIW-based configuration and the incorporation of the meandered slot line, the filter occupies an area of $0.041\lambda_g^2$ at the center frequency of the first passband (4.7 GHz). Compared with previously reported SIW-based multi-band filters, the proposed design achieves a significantly reduced footprint while maintaining satisfactory filtering performance. To verify the proposed design, two independent full-wave electromagnetic simulation platforms were employed. The primary design and optimization procedures were carried out using Ansys Electronics Desktop (EDT) 2022 R1. In addition, ADS 2020 was utilized as a secondary simulation environment to validate the obtained results and ensure consistency between different numerical solvers. The simulated insertion-loss responses obtained from both software packages are presented in Fig. 9(a). Excellent agreement can be observed between the two sets of results, confirming the reliability of the proposed design methodology. The filter exhibits three passbands centered at 4.7 GHz, 7.28 GHz, and 9.36 GHz. The corresponding fractional bandwidths (FBWs) are 17.08%, 5.79%, and 2.46%, respectively. In terms of selectivity, the filter provides an isolation level of approximately 16 dB between the first and second passbands, while the isolation between the second and third passbands reaches 26.5 dB. Furthermore, an upper stopband suppression better than 20 dB is maintained over the frequency range from 9.68 GHz to 16 GHz, demonstrating effective out-of-band rejection characteristics.

The insertion losses at the center frequencies of the three operating bands are 0.23 dB, 0.77 dB, and 1.8 dB, respectively. These low-loss characteristics, together with the compact size and multi-band operation, highlight the suitability of the proposed filter for modern wireless communication applications.

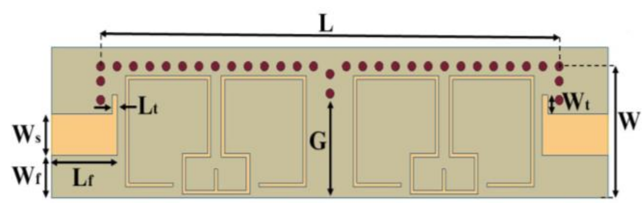

Figure 8. Proposed 2nd order HMSIW BPF.

The simulated return-loss (RL) response of the proposed filter is presented in Fig. 9(b). The obtained results indicate excellent impedance matching across the three operating bands, with return-loss values exceeding 20 dB in the first passband, 19 dB in the second passband, and 18 dB in the third passband. To further verify the accuracy of the design, the insertion-loss and return-loss responses generated using Ansys EDT were compared with those obtained from ADS simulations. A close correlation between the two sets of results was observed, with only minor discrepancies. These differences can be attributed to the distinct electromagnetic modeling approaches adopted by the simulators, particularly the superior capability of the 3D Ansys environment in accurately representing vertical structures such as metallic vias.

Table 3. The Dimensions of the suggested filter in (mm).

Variables	Dimension	Variables	Dimension	Variables	Dimension
L	7	A_3	1.45	B_4	0.57
W	3.5	A_4	0.77	W_f	1.136
d	0.25	A_5	0.32	L_f	2.02
P	0.5	S	0.1	W_s	01.1
h	0.508	B_1	2.75	G	2.65
A_1	2.06	B_2	2	L_t	0.175
A_2	2.6	B3	1.1	W_t	0.5

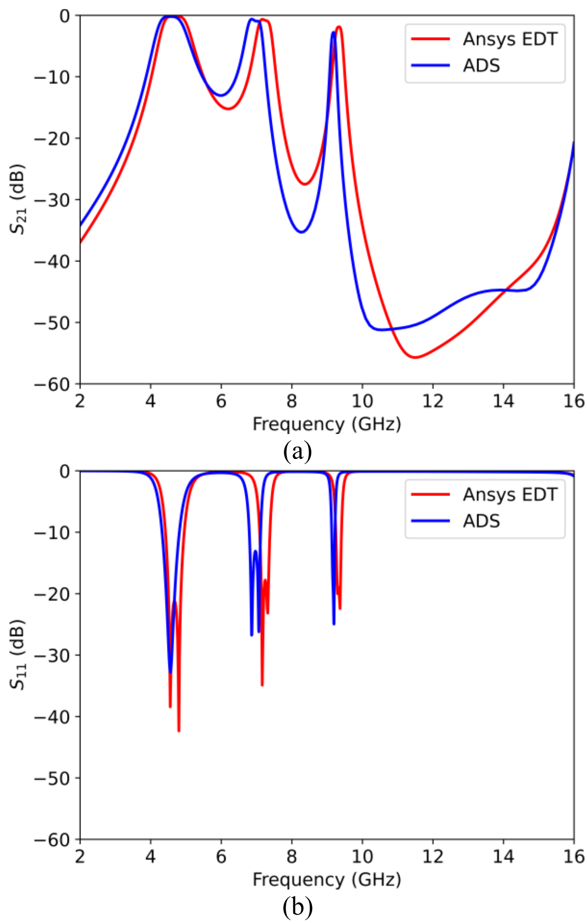

Figure 9. Simulation results of the suggested filter with two full-wave simulators (a) S_{21} and (b) S_{11}.

The electric-field distributions were examined at several representative frequencies to give further insight into how the filter operates. Fig. 10(a)-(g) show the field patterns at 2, 4.7, 6.2, 7.28, 8.35, 9.36 and 11.5 GHz. At the center frequencies of the three passbands, 4.7, 7.28 and 9.36 GHz, the energy travels efficiently from the input port to the output port with little reflection, as seen in Figs. 10(b), 10(d) and 10(f). At 2, 6.2, 8.35, and 11.5 GHz, the picture is different: the field stays confined near the input and is strongly reflected, which corresponds to the stopband regions of Figs. 10(a), 10(c), 10(e) and 10(g). These field distributions provide clear physical evidence of the filtering mechanism and confirm the proper operation of the proposed tri-band structure.

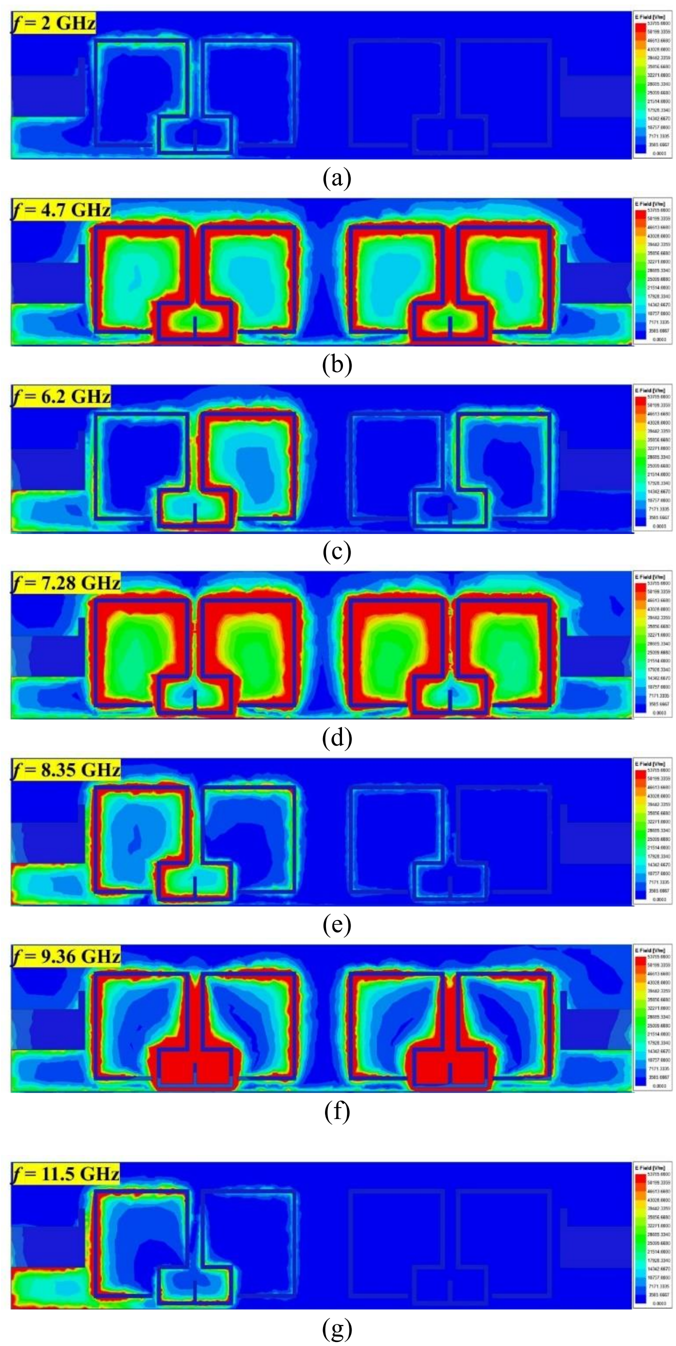

Figure 10. Electric-field distribution at different frequencies in GHz: (a) 2, (b) 4.7, (c) 6.2, (d) 7.28, (e) 8.35, (f) 9.36, and (g) 11.5.

The tuning capability of the filter was further investigated through a set of parametric studies. The results, presented in Fig. 11, demonstrate the influence of selected geometrical parameters on the passband locations. As shown in Fig. 11(a), increasing B1 shifts all three passbands toward lower frequencies, with the first passband exhibiting the highest sensitivity. Fig. 11(b) reveals that variations in B3 primarily affect the second and third passbands, while the first passband remains nearly unchanged. A similar trend is observed for parameter B4, as depicted in Fig. 11(c), where the second and third passbands experience noticeable downward shifts with only negligible influence on the first passband. The effect of A5 is illustrated in Fig. 11(d), showing significant tuning of the first and third passbands, whereas the second passband undergoes comparatively smaller changes.

These results demonstrate that the proposed filter offers multiple tuning degrees of freedom, enabling effective adjustment of the operating bands with limited mutual interaction. Consequently, the filter can be tailored to different frequency allocations while maintaining quasi-independent control of the three passbands, making it a flexible solution for multi-band wireless communication systems.

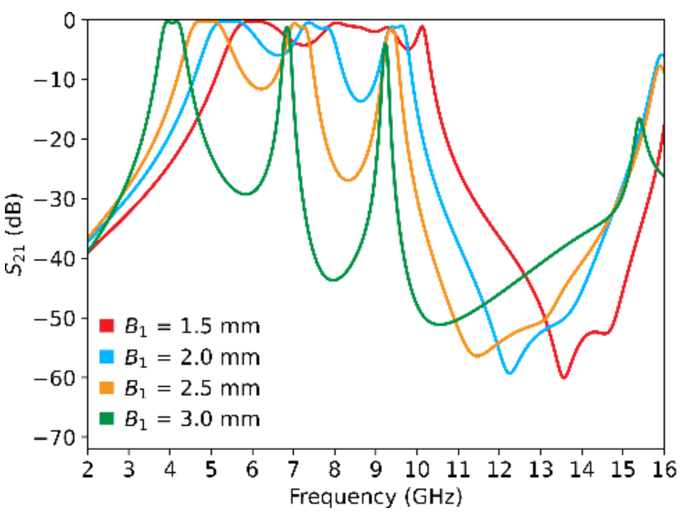

(a)

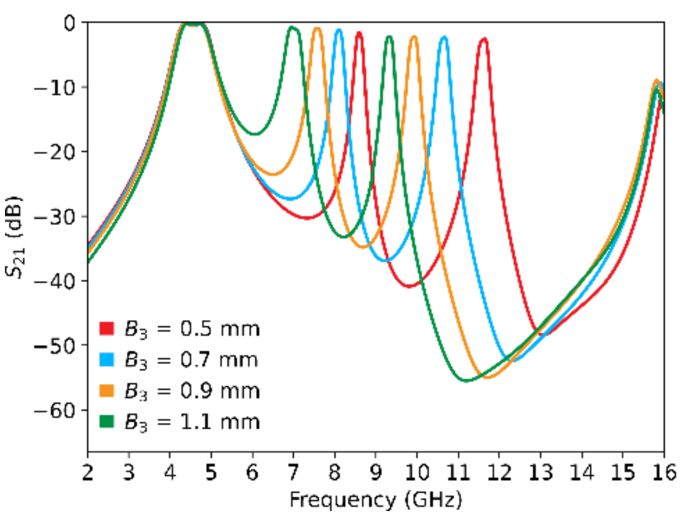

(b)

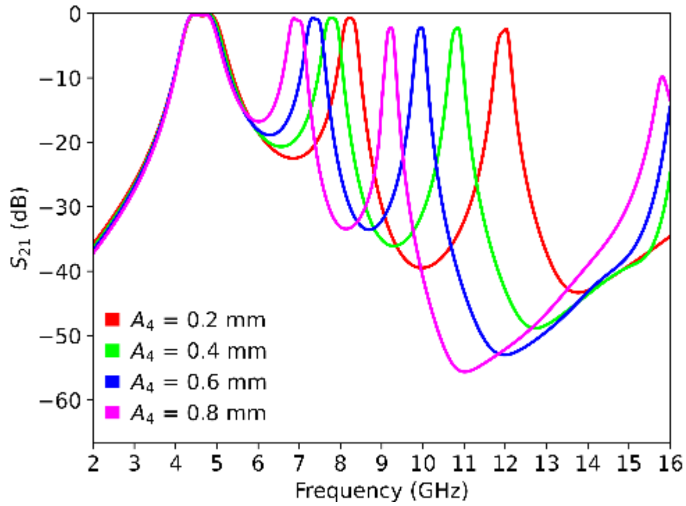

(c)

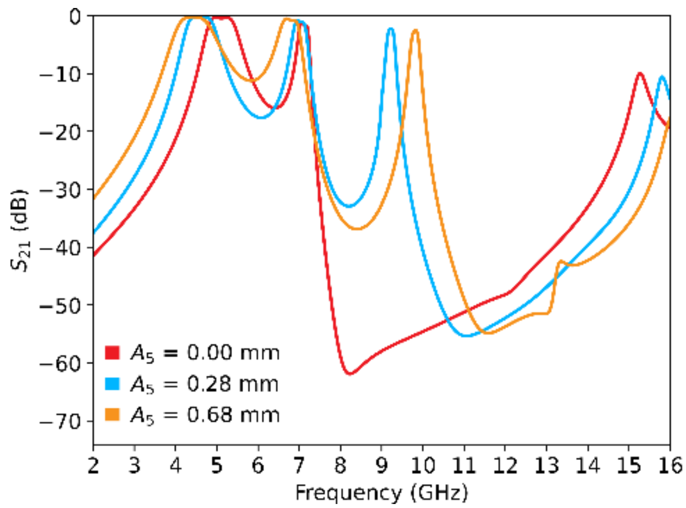

(d)

Figure 11. S_{21} at different parameters (a) B_1, (b) B_3, (c) A_4, and (d) A_5.

Table 4 presents a performance comparison between the proposed tri-band bandpass filter and recently reported SIW-based tri-band filters. For a fair evaluation, only second-order filter designs are considered. As observed from the comparison, the proposed filter achieves the smallest footprint among the listed structures while maintaining effective tri-band operation with a high degree of frequency-tuning flexibility. The quasi-independent control of the operating bands further enhances its suitability for contemporary multi-band wireless communication systems. In addition to its compact size, the proposed design offers competitive filtering characteristics when compared with previously reported counterparts. The achieved miniaturization is primarily attributed to the combination of the HMSIW cavity and the meandered slot-line loading technique, which significantly reduces the resonator dimensions without sacrificing the desired filtering response. It should be noted that the reported performance metrics are based on full-wave electromagnetic simulations. Consequently, the relatively low insertion-loss values represent ideal simulated conditions and may increase slightly in a fabricated prototype due to practical factors such as conductor losses, dielectric losses, fabrication tolerances, and connector effects.

Table 4. Comparison of the suggested filter with relevant research.

Ref.	Mini. Method*	f_0 (GHz)	FBW (%)	IL (dB)	RL (dB)	Size (λ_g^2)	Ind.*
		13	4.06	1.7			
[18]	via-post SIW	14	3.31	1.8	8	4.02	No
		15	2.82	2.29			
		16.9	1.22	2.53			
[19]	via-post SIW	17.5	2.43	1.23	16.9	2.07	Yes
		21.3	2.98	1.31			
[20]		1.83	3.01	2.31			
	Circular SIW	2.1	2.86	3.01	15	0.048	No
		2.47	2.31	2.25			
		11.92	2.85	1.81			
[21]	via-post SIW	13.23	1.29	2.35	15	2.72	No
		14.1	1.42	1.93			
		12.7	9.5	1.6			
[22]	HM SIW	20.7	6.2	2.5	13	0.12	Yes
		28.6	4.5	2.2			
		2.1	17.1	0.93			
[23]	QM SIW	3.98	8.8	0.98	15	0.1	No
		6.6	8.4	1.2			
		3	3.7	3.24			
[24]	TFM SIW	4.24	5.1	2.2	15	1.07	No
		5.24	3.8	2.85			
		4.7	17.08	0.23			
T.W	MSL HMSIW	7.28	5.79	0.77	15	0.041	Yes
		9.36	2.46	1.8			

*where Mini. refers to miniaturization, Ind. means independence, and T. W represents this work.

5. Conclusions

This paper presented the design and analysis of a compact tri-band BPF by integrating MSL on HMSIW. The suggested filter is second-order with quasi-independent passbands, where this functionality was obtained by employing various parameters of the MSL; moreover, the MSL acts as a miniaturization degree of freedom.

Since the suggested solution was developed on affordable printed circuit board planner technology with a multifunctionality filtering response, the proposed filter can be seen as an excellent candidate for modern and emerging wireless communication systems. The proposed operating bands can be easily adjusted to suit different and future applications, where a systematic design procedure was utilized, allowing flexible controllability over center frequencies, filter order, and FBWs.

Two full-wave simulators were utilized in this work to design, analyze, optimize, and validate the suggested filter. Simulation results revealed that the proposed structure has a low insertion loss, especially in the first two bands, high impedance matching with RL > 15, and a high rejection level in the stopband, with rejection better than 20 dB over the frequency range of 9.68 GHz to 16 GHz. Comparing the footprint of the proposed design, which occupied a small area of $0.041\lambda_g^2$, with state-of-the-art SIW-based tri-band BPF, it shows a better filtering response and superior performance.

Acknowledgements

This work was supported in part by the University of Technology- Iraq and the Iraqi Ministry of Higher Education and Scientific Research.

Conflict of interest

The authors declare that there are no conflicts of interest regarding the publication of this manuscript.

Author Contribution Statement

Hasan Al-Darraji: conceptualized the idea and outlined the main concepts. He conducted the theoretical analyses, executed the full-wave simulators (Ansys EDT and ADS), and drafted the manuscript.

Hussam Al-Saedi: contributed to the planning and supervision of the work. He assisted in interpreting the results and contributed to the revision of the manuscript.

References

[1] Q. Liu, D. Zhou, X. Wang, M. Tang, D. Zhang, and Y. Zhang, "High-Selective Bandpass Filters Based on New Dual-Mode Rectangular Strip Patch Resonators," *IEEE Microw. Wirel. Components Lett*., vol. 31, no. 10, pp. 1123–1126,2021. https://doi.org/10.1109/LMWC.2021.3106128

[2] Y. Zhan, Y. Wu, E. Fourn, P. Besnier, and K. Ma, "Synthesis and Implementation of Multiband SIW Bandpass Filters Based on In-Line Topology," *IEEE Trans. Microw. Theory Tech.*, vol. 72, pp. 6623–6636, 2024. https://doi.org/10.1109/TMTT.2024.3392890.

[3] A. Iqbal, J. J. Tiang, S. K. Wong, M. Alibakhshikenari, F. Falcone, and E. Limiti, "Miniaturization Trends in Substrate Integrated Waveguide (SIW) Filters: A Review," *IEEE Access*, vol. 8, pp. 223287–223305, 2020. https://doi.org/10.1109/access.2020.3044088

[4] H. Al-Saedi, J. Al Attari, W. M. A. Wahab, R. Mittra, and S. Safavi-Naeini, "Single-feed Dual-band Aperture-coupled Antenna for 5G applications," Proc. - ANTEM 2018 2018 18th Int. Symp. Antenna Technol. Appl. Electromagn., 2018-August, pp. 1–2, 2018. https://doi.org/10.1109/ANTEM.2018.8572907.

[5] N. T. Nguyen, N. Shlezinger, Y. C. Eldar, and M. Juntti, "Multiuser MIMO Wideband Joint Communications and Sensing System with Subcarrier Allocation," *IEEE Trans. Signal Process*., vol. 71, pp. 2997–3013, 2023. https://doi.org/10.1109/TSP.2023.3302622.

[6] H. I. Khani, A. S. Ezzulddin, and H. Al-Saedi, "Design of High-Selectivity Compact Quad-Band BPF Using Multi-Coupled Line and Short Stub-SIR Resonators," *Progress in Electromagnetics Research*. vol. 122, no. May, pp. 215–228, 2022. https://doi.org/10.2528/pierc22052903

[7] K. Zhao and D. Psychogiou, "Three-Dimensional Printed Vertically-Stacked Single-/Multi-Band Coaxial Filters and RF Diplexers," *IEEE Trans. Microw. Theory Tech*., vol. 71, no. 11, pp. 4957–4968, 2023. https://doi.org/10.1109/TMTT.2023.3269522.

[8] H. Zhang, W. Kang, and W. Wu, "Miniaturized Dual-Band SIW Filters Using E-Shaped Slotlines with Controllable Center Frequencies," *IEEE Microw. Wirel. Components Lett.*, vol. 28, no. 4, pp. 311–313, 2018. https://doi.org/10.1109/LMWC.2018.2811251

[9] H. Zhang, W. Kang, and W. Wu, "Dual-band substrate integrated waveguide bandpass filter utilising complementary split-ring resonators," *Electron. Lett.*, vol. 54, no. 2, pp. 85–87, 2018. https://doi.org/10.1049/el.2017.3478

[10] A. R. Azad and A. Mohan, "Single- and Dual-Band Bandpass Filters Using a Single Perturbed SIW Circular Cavity," *IEEE Microw. Wirel. Components Lett.,* vol. 29, no. 3, pp. 201–203, 2019. https://doi.org/10.1109/LMWC.2019.2893379

[11] Y. Liu, G. Zhang, and J. Zheng, "Compact dual-band balanced SIW bandpass filter with two adjustable closed-passbands," *Electron. Lett.*, vol. 56, no. 13, pp. 667–669, 2020. https://doi.org/10.1049/el.2020.0576

[12] H. W. Xie, K. Zhou, C. X. Zhou, and W. Wu, "Compact SIW Diplexers and Dual-Band Bandpass Filter with Wide-Stopband Performances," *IEEE Trans. Circuits Syst. II Express Briefs*, vol. 67, no. 12, pp. 2933–2937, 2020. https://doi.org/10.1109/TCSII.2020.2992059.

[13] M. F. Abbas and A. J. Salim, "A New Tunable Dual-Mode Dual-Band Square Cavity SIW Bandpass Filter," *Prog. Electromagn. Res.* C, vol. 118, no. January, pp. 113–123,2022. https://doi.org/10.2528/PIERC21120306.

[14] F. Zhu, Y. Wu, P. Chu, G. Q. Luo, and K. Wu, "Compact Dual-Band Filtering Baluns Using Perturbed Substrate Integrated Waveguide Circular Cavities," *IEEE Microw. Wirel. Technol. Lett.*, vol. 33, no. 6, pp. 663–666, 2023. https://doi.org/10.1109/lmwt.2023.3243646

[15] Z. Yang, B. You, and G. Luo, "Dual−/tri-band bandpass filter using multimode rectangular SIW cavity," Microwave and Optical Technology Letters, vol. 62, no. 3, pp. 1098–1102, 2020. https://doi.org/10.1002/mop.32145.

[16] D. Li, W. Luo, X. Chen, Y. Liu, K. Da Xu, and Q. Chen, "Miniaturized Dual-/Tri-/Quad-Band Bandpass Filters Using Perturbed Multimode SIW Cavity," *IEEE Trans. Components, Packag. Manuf. Technol*., vol. 13, no. 10, pp. 1685–1693, 2023. https://doi.org/10.1109/TCPMT.2023.3311439.

[17] Q. Li, "Design of Miniaturized Multiband Substrate Integrated Waveguide Filters," 2023 5th Int. Conf. Commun. Inf. Syst. Comput. Eng. CISCE 2023, pp. 94–97, 2023. https://doi.org/10.1109/CISCE58541.2023.10142576.

[18] H. W. Xie, K. Zhou, C. X. Zhou, and W. Wu, "Substrate-Integrated Waveguide Triple-Band Bandpass Filters Using Triple-Mode Cavities," *IEEE Trans. Microw. Theory Tech*., vol. 66, no. 6, pp. 2967–2977, 2018. https://doi.org/10.1109/TMTT.2018.2833462

[19] Y. J. Liu, G. Zhang, S. C. Liu, and J. Q. Yang, "Compact triple-band filter with adjustable passbands on one substrate integrated waveguide square resonant cavity," *Microw. Opt. Technol. Lett.,* vol. 62, no. 12, pp. 3709–3715, 2020. https://doi.org/10.1002/mop.32491.

[20] M. H. Ho and K. H. Tang, "Miniaturized SIW Cavity Tri-Band Filter Design," *IEEE Microw. Wirel. Components Lett*., vol. 30, no. 6, pp. 589–592, 2020. https://doi.org/10.1109/LMWC.2020.2987172.

[21] D. Li, X. Chen, W. Luo, Z. Zheng, and Q. Chen, "Compact Tri-Band SIW Bandpass Filters with High Selectivity and Controllable Center Frequencies Using Perturbation Structure," *IEEE Trans. Circuits Syst. II Express Briefs,* vol. 70, no. 11, pp. 4043–4047, 2023. https://doi.org/10.1109/TCSII.2023.3281496.

[22] S. Pelluri and M. V. Kartikeyan, "Compact triple-band bandpass filter using multi-mode HMSIW cavity and half-mode DGS," I*nt. J. Microw. Wirel. Technol.*, vol. 13, no. 2, pp. 103–110, 2021. https://doi.org/10.1017/S1759078720000902

[23] A. Iqbal, J. J. Tiang, S. K. Wong, S. W. Wong, and N. K. Mallat, "QMSIW-Based single and triple band bandpass filters," IEEE Trans. Circuits Syst. II Express Briefs, vol. 68, no. 7, pp. 2443–2447, 2021. https://doi.org/10.1109/TCSII.2021.3055904

[24] L.-Y. Weng and W.-H. Tu, "Three-fourths-mode substrate-integrated waveguide for tri-band bandpass filter," *Microw. Opt. Technol. Lett.,* vol. 66, no. 1, no. e34032, 2024, https://doi.org/10.1002/mop.34032

[25] X. P. Chen and K. Wu, "Substrate integrated waveguide filter: Basic design rules and fundamental structure features," *IEEE Microw. Mag.,* vol. 15, no. 5, pp. 108–116, 2014. https://doi.org/10.1109/MMM.2014.2321263

[26] Q. Lai, C. Fumeaux, W. Hong, and R. Vahldieck, "Characterization of the propagation properties of the half-mode substrate integrated waveguide," *IEEE Trans. Microw. Theory Tech.*, vol. 57, no. 8, pp. 1996–2004, 2009. https://doi.org/10.1109/TMTT.2009.2025429

[27] R. J. Cameron, C. M. Kudsia, and R. R. Mansour, *Microwave Filters for Communication Systems: Fundamentals, Design, and Applications*, 2nd ed. Hoboken, NJ, USA: Wiley, 2018. https://lccn.loc.gov/2006036928